*And., Intl.,J., Appl Sci., Eng., Tech, Vol 04, No 02, July 2024*
*e-ISSN: 2797-0442*

# Hybrid Ag@Rice Leaf Biochar Nanocomposite as Photocatalyst for Efficient Degradation of Methylene Blue and Denaturation of Micro-Organisms

**Nworie Felix Sunday[1], Nwabue Frank[1], Elom Meashack[1], Oroke Clinton[2], Oke Boniface[3], Eze Nkechi[1], and Ike-Amadi Chioma[4]**
[1]Department of Industrial Chemistry, Ebonyi State University, Abakaliki, Nigeria
[2]Department of Science Technology, Federal Polytechnic Ado Ekiti, Nigeria
[3]Department of Microbiology, Ebonyi State University, Abakaliki, Nigeria
[4]Department of Chemistry Abia State polytechnic, Abia State, Nigeria
[*]Corresponding author, e-mail: nworie.sunday@ebsu.edu.ng

**Abstract**— Organic-inorganic hybrid nanocomposite is currently in the fore front of research because it is ecofriendly, safe, cost effective, methodologically facile and effective for the removal of methylene blue (MB) from aqueous solution. In this study, hybrid Ag@rice leaf extract/rice leaf biochar nanocomposite (Ag@RLEBN) was hydrothermally fabricated for the degradation of MB and denaturation of microorganisms. To understand the mechanisms between Ag@RLEBN and MB/microorganism, the physicochemical analysis, reusability, photocatalytic degradation parameters and microbial inhibition diameter were investigated. The obtained results revealed Ag@RLEBN as face centered cubic crystalline structure with crystallite size of 27.5 nm. The band gap energy of rice leaf biochar (RLB) and Ag@RLEBN was 1.9 and 1.8 eV respectively. Photocatalytic degradation of 99.7% was obtained at initial MB concentration of 0.0001M, 5 mg of Ag@RLEBN and 60 min exposure to sunlight. The main mechanism in control of the degradation of MB was electrostatic attraction, complexation, cationic exchange, π–π, n–π, and hydrogen bonding. Accessing the reusability of Ag@RLEBN indicated less than 2.05% degradation efficiency disparity after five cycle reuse. The Ag@RLEBN showed high antimicrobial inhibition effectiveness against salmonella (10 nm), Klebsiella (12 nm) and staph aureus (8nm). Therefore, Ag@RLEBN is effective for the removal of MB and microbial decontamination.

*Keywords: rice leaf, biochar; nanocomposite, photocatalyst, antimicrobial, methylene blue, degradation, denaturation, micro-organism.*



## 1. Introduction

In recent years, the development of novel bioinspired nanocomposite materials with advanced properties has gained significant attention due to their diverse applications in various fields. Nanocomposites, have emerged as promising candidates owing to their unique combination of properties derived from their constituent materials [1]. Among these, the synthesis and study of biochar-based nanocomposites have attracted considerable interest due to their eco-friendly nature and potential for sustainable applications. Nanocomposites, which consist of nanoparticles embedded in a matrix material, exhibit enhanced properties and functionalities compared to their bulk counterparts [2-4]. This has led researchers to explore their potential for various applications, including environmental remediation and antimicrobial therapies. The incorporation of rice leaf extract and silver nanoparticles into the rice leaf biochar matrix generates hybrid nanocomposite with enhanced structural –physical and dynamics properties a consequence of the synergistic effect of the components. The improved properties lead to enhanced photocatalytic and antimicrobial activity due

*Received: April 30, 2024, Revised: June 16, 2024, Accepted: June 22, 2024*
*https://doi.org/10.25077/aijaset.v4i2.134*

to sustained and gradual release of silver ions from the biochar matrix.

Biochar, a carbon-rich material derived from the pyrolysis of organic biomass, has shown promising properties as an adsorbent, catalyst, and support matrix for the integration of nanoparticles. One such nanoparticle of significant interest is silver (Ag) plant extract based, renowned for its excellent photocatalytic and antimicrobial properties. The integration of silver nanoparticles into biochar matrices has opened up new possibilities for harnessing the combined benefits of both materials. Biochar is known for its high surface area and porosity, which can be beneficial for adsorption and catalytic reactions [1-5]. The rice leaf biochar serves as an ideal support matrix due to its porous structure, low cost, renewable availability, large surface area, and renewable nature, making it an eco-friendly alternative to conventional carbon sources.

Rice (Oryza sativa) is one of the most widely cultivated cereal grains and a staple food for a large part of the world's population [6]. While rice grains are the primary part of the plant consumed for nutrition, various other components of the rice plant, including the leaves, contain bioactive compounds with potential benefits. The extract from rice leaves may contain a variety of compounds, such as antioxidants for neutralizing harmful free radicals in the body and phytochemicals such as phenols, flavonoids and other bioactive substances [7]. These substances exert anti-inflammatory, moisturizing, soothing and anti-aging properties [7]

Methylene blue is a common dye used in various industries and a medication with various applications. It can be found in laboratories, medical settings, and even used as a treatment for certain medical conditions [8-10]. Methylene blue is known for its blue color and is harmful to the environment if released without proper treatment. Some side effects of methylene blue include headache, dizziness, nausea, and vomiting [11-13]. The removal of methylene blue has been achieved by chemical precipitation, ion exchange and adsorption methods [9,14]. These methods suffer one or more defects such as high cost, disposal problems, unsafe by-product and wastage of time. In this study, the use of photocatalyst of silver rice leaf extract nanoparticles decorated on rice leaf biochar surface facilitates a chemical reaction under the influence of light. When light is absorbed by the catalyst, it initiates reactions with the target pollutant; the methylene blue and generates reactive species like hydroxyl radicals. These reactive species then break down the methylene blue into less harmful substances like water and carbon dioxide [2]. By utilizing this nanocomposite as a photocatalyst, it becomes possible to efficiently and cost-effectively remove organic pollutants (methylene blue) from wastewater before discharging it into the environment.

The emergence of drug-resistant microorganisms has become a major global concern, underscoring the urgency for novel antimicrobial agents. Silver nanoparticles have exhibited strong antimicrobial properties against a wide range of bacteria, fungi, and viruses [15-16]. By incorporating silver nanoparticles into rice leaf biochar, the resulting silver rice leaf biochar nanocomposite demonstrates potent antimicrobial activity. The nanocomposite's unique structure of small size and high surface area allows for controlled release of silver ions, which disrupt the cellular membranes and enzymatic processes of microorganisms, leading to their inactivation, and ultimately, cell death [17].

In this study, the silver rice leaf biochar nanocomposite was synthesized under hydrothermal condition and applied for the removal of methylene blue from solution and as antimicrobial agent for the decimation of tested pathogenic organisms.

## 2. Method

Silver nitrate (99.8%) and methylene blue were sourced from Sigma Aldrich

### 2.1 Haracterization of Biochar and Nanocomposite

Different techniques such as UV-Visible spectroscopy, fourier transform infrared spectroscopy, x-ray diffraction, scanning electron microscopy and energy dispersive spectroscopy were used for the

physicochemical characterization of the biochar and nanocomposite. The surface Plasmon resonance of biochar and Ag@RLEBN was determined using UV-visible (UV-VIS) spectroscopy (Uv –visible spectrophotometer, Model. 721), The functional group present in the biochar and nanocomposite and type of bonding interaction was evaluated using fourier transform infrared (FTIR) spectroscopy (FTIR spectrometer, Andor,Model. SR 5OOi). The morphologies and elemental compositions were characterized using scanning electron microscopy fitted with energy dispersive (EDX) Spectrometer. (Shimadzu, model. EDX 7200). X-Ray diffraction (XRD) was carried out on a Shimadzu XRD-7000 X-ray diffractometer using Cu Kα radiation (λ = 0.15418 nm) at a scanning rate of 2° $min^{-1}$ in a 2θ range of 5° - 70°. The phase crystallinity was evaluated using Eq 1 [18].

$$d = \frac{K\lambda}{\beta Cos\theta} \quad (1)$$

Where K is Debye-Scherer constant, β is the full width at half maximum, λ is the wavelength and θ is Bragg angle.

### 2.2 Sample Collection/Preparation

Fresh, tender and rice leaves of two months from date of plantation were collected from a farmland in Ebonyi State University main campus. The rice leaves were washed severally with distilled water, sun dried to reduce moisture content for 7 days and pulverized. Exactly 20 g of the powdered sample was measured and dissolved in 400 mL of distilled water and then, heated with stirring at 80ºC for 30 min. The solution was allowed to cool, filtered and kept at 4 ºC for further use.

### 2.3 Preparation of Rice Leaf Biochar (RLB)

Dried rice leaves were carbonized at temperature of 500ºC for 30 min to produce the rice leaf biochar (RLB). The produced RLB was then ground and kept in airtight container for further use.

### 2.4 Synthesis of Ag-rice Leaf Extracts Biochar Nanocomposite (Ag@RLEBN)

In the synthetic process, 7.9 g of pulverized RLB was dispersed into 100 mL of distilled water followed with 100 mL of the rice leaf extract and 0.158g of AgNO3 solution. The solution was stirred and heated at 80oC for 30min to reduce the silver ions on the surface of the RLB so as to obtain the silver-rice leaf extracts biochar nanocomposite (Ag@RLEBN). The mixture after 30 min was allowed to cool and centrifuged. The obtained nanocomposite was then washed repeatedly with ethanol and then with distilled water, dried in an oven at 110oC for 1hr and then kept for further use.

### 2.5 Photocatalytic Studies

The Photocatalytic experiment was done in four different ways; (a) concentration variation (b) time variation (variation of dosage of nanocomposite and (d) Desorption and reusability studies using nitric acid for desorbing the adsorbed MB and then followed with reuse of the catalyst. The percentage degradation of MB for each of the methods was calculated using Eq 2 [19].

$$\%Degradation = Ao/A \times 100 \quad (2)$$

Where; Ao = Absorbance of the control , A = absorbance of solution.

#### 2.5.1 Variation of initial concentration of MB

In this study, 0.05g of Ag@RLEBN was measured into four different sample bottles and 0.05g of the RLB was also measured into the fifth sample bottle, serving as the control. Then, 10 mL of different concentrations of MB (0.1 to 0.0001M) was added to the four separate sample bottles containing the nanocomposite whereas the bottle with the RLB (control) was added 10 mL of 0.001 M MB. The five sample bottles were agitated for 30 min in the dark and kept under the sun light for 60 min. These were thereafter filtered and centrifuged at 17000 rpm and the UV of the supernatant was read at 640 nm against blank.

#### 2.5.2 Variation of time of exposure of MB and photocatalyst to sunlight

The process involves measurement of 0.05g of Ag@RLEBN into five different sample bottles and 0.05g of RLB into another sample bottle to serve as control. Then, 10 mL of 0.001M of MB was

added to each of the sample bottles. The sample bottles containing Ag@RLEBN/MB or RLB/MB were agitated for 30 min under the dark before taking them to sunlight. Thereafter, the samples were picked out of the sun at regular intervals of 20, 40, 60, 80 and 100 min respectively for the five sample bottles containing Ag@RLEBN/MB while the sample bottle containing RLB/MB (control) was removed at 60 min. The solutions were filtered and then centrifuged at 17000 rpm and the absorbance of the supernatant taken at 640 nm against blank.

### 2.5.3 Variation of dosage of Ag@RLEBN

The effect of dosage of Ag@RLEBN on MB degradation was studied using different doses of the photocatalyst at range of 0.001 to 0.008g at 60 min of photocatalytic activity and 0.001M solution of MB. The solutions of different doses in separate sample bottles were treated by allowing them under the dark for 30 min with stirring and thereafter exposed to sunlight for 60 min. The solutions filtered and then centrifuged at 17000 rpm and the absorbance of the supernatant taken at 640 nm against blank.

### 2.5.4 Desorption/ recovery/ reuseability studies

The recovery studies were effected by measuring 0.05g of MB loaded Ag@RLEBN into three different sample bottles while the fourth bottle contains the blank (MB loaded RLB). Then 10 mL of different concentrations of $HNO_3$ (0.1M, 0.01M and 0.001M) was added to each of the three samples respectively. All the samples were agitated simultaneously for 30 min centrifuged at 17000 rpm and the UV of the supernatant determined at 640 nm against blank. The recovered Ag@RLEBN was dried and reused for the photocatalytic removal of MB. This was done for five different times maintaining all conditions for the photocatalytic process.

## 2.6 Evaluation of the Antimicrobial Activity of Ag@RLEBN and RLB

The antibacterial performance of the fabricated Ag@RLEBN and RLB against selected organisms (gram positive and gram negative); Salmonella spp., Escherichia. coli, Klebsiella spp. and Staphylococcus aureu was performed using the agar well diffusion approach. The bacterial isolates were cultured for 20 hours at 35°C in a medium of nutritional broth having 10 g/L NaCl, 3 g/L extract of yeast, and 8 g/L bactotryptone. Using sterile cotton buds, 100 µL of the suspensions of the cell was dispersed on a nutrient agar surface, and the agar was pierced with 8 mm diameter reservoirs and loaded with 300 µL of Ag@RLEBN or RLB aqueous solutions (5 mg/mL). The plates were incubated for 24 h at 35°C and the antibacterial performance of Ag@RLEBN and RLB was assessed by the size of the inhibition zone [19].

# 3. Result and Discussion

## 3.1 Characterization of RLB and Ag@RLEBN Samples

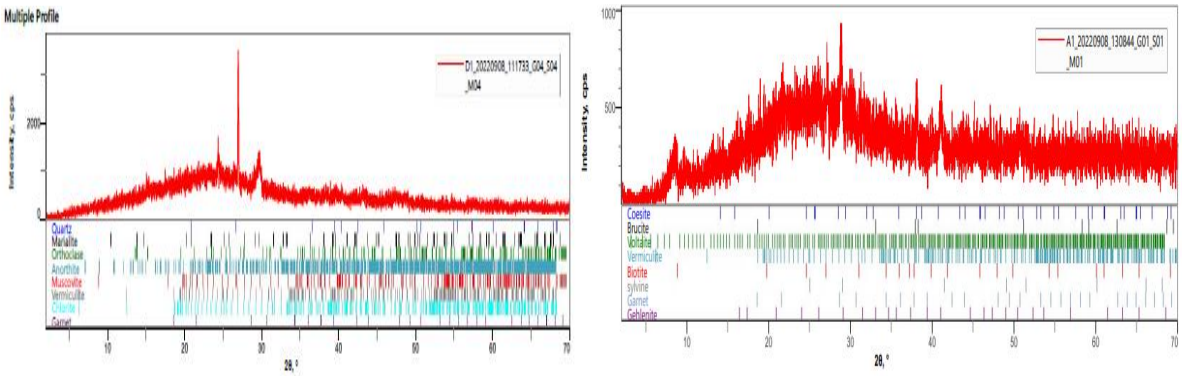


**Figure 1.** X-ray diffraction pattern of A (RLB) and, B (Ag@RLEBN)

The x-ray diffractogram shown in Figure 1 for RLB illustrated sharp peaks an indication of the high crystalline, high surface area and nanostructured form of the biomaterial. The diffraction peaks were observed at 2θ values of 24°, 26° and 28° corresponding to the reflection patterns of (110),

(011) and (220) respectively. The formation of the nanocomposite Ag@RLEBN was depicted by diffraction peaks observed at 2θ values of 26°, 28°, 32°, 38°, 42°, 52° corresponding to the reflection patterns of (011 ), (220 ), (400 ), (111 ) (422 ) and ( 511 ) respectively and refers to face-centred cubic silver(JCPDS file number: 040783) as previously noted by other researchers for Ag-biochar composites [20]. The emergence of the (111) plane is consistent with the preferred growth pattern of Ag-biochar nanocomposites biosynthetically fabricated according to previous studies [21-22]. The observed peak shift to highest angles owing to the immobilization of the Ag and the interaction with the solid matrix biochar introduces strain and alteration in the chemical constituent of the nanocomposite. As a consequence of the introduction of $AgNO_3$, there was hydrogen bond cleavage, good interaction of Ag ions with biochar, increased surface area and peak broadening of the nanocomposite. Evaluating the crystallite size from equation 1, indicated 24.1 and 27.5 nm respectively for the RLB and Ag@RLEBN.

### 3.2 FTIR Spectra of RLB, Ag@RLEBN and MB- Loaded Ag-RLEBN

The FTIR spectra of RLB, Ag@RLEBN and MB-loaded Ag@RLEBN as shown in Figure 2 A, B and C respectively was recorded at the region of 4000-400 $cm^{-1}$. The MB-loaded Ag@RLEBN has peak at 3652.8 $cm^{-1}$ corresponding to rocking or wagging vibration of water molecules. The peak at 3034.1 $cm^{-1}$ for the RLB shifted to 3250.1 $cm^{-1}$ in the Ag@RLEBN and then to 3276.3 $cm^{-1}$ for the MB-loaded Ag@RLEBN. These peaks indicate the stretching vibration of –OH group which may be connected with the water molecules in the biochar and nanocomposite and inter or intra hydrogen bonding interaction [23]. The difference between the peaks for RLB and Ag@RLEBN is 242.2 $cm^{-1}$ an indication that complexation is highly evident in the impregnation of Ag onto the rice leaf extract /biochar. The peaks observed at 1871.1 $cm^{-1}$ for RLB and which decreased to 1561.8 $cm^{-1}$ for both Ag@RLEBN and the MB loaded nanocomposite was assigned to symmetric and asymmetric vibration of carboxyl group. The difference between the peaks of RLB and Ag@RLEBN is 310 $cm^{-1}$ signifying that cationic exchange is prominent. The peaks at 779.0 $cm^{-1}$ was assigned to Ag-O stretching vibration and corresponds to the face-centred cubic structure of silver [1].

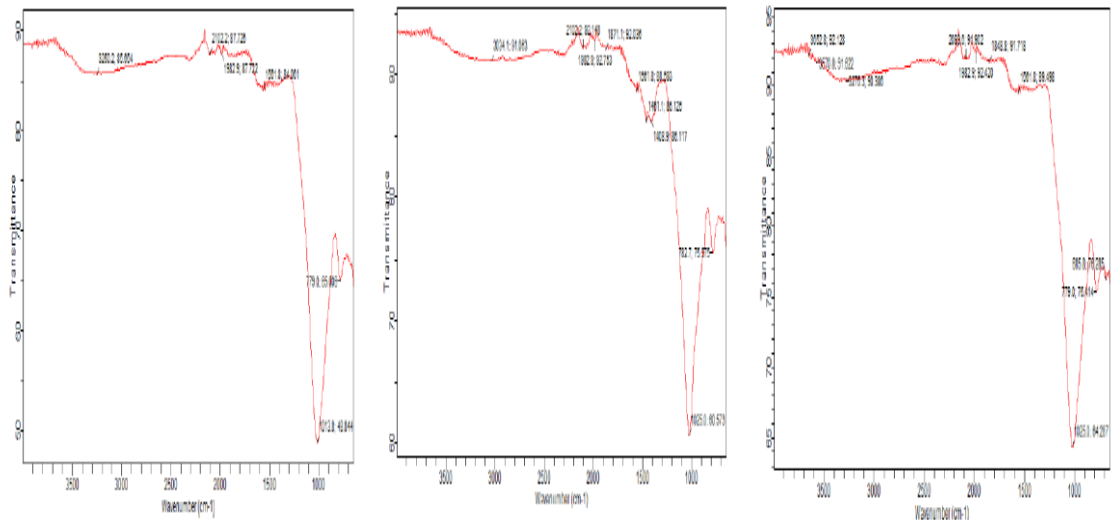

**Figure 2.** FTIR spectra bands of (A) RLB , (B) Ag@RLEBN (C) MB-loaded Ag@RLEBN

### 3.3 UV-Visible Spectroscopy

The UV-Vis analysis of RLB and Ag@RLEBN indicated surface Plasmon resonance peak 550 and 650 nm (Figures 3A and B) respectively which was within the range reported by other workers [1]. The band gap energy (Eg) evaluated using Equ (2)[1] of RLB and Ag@RLEBN was 1.9 and 1.8 eV respectively. The band energy gap of RLB was higher than that of Ag@RLEBN because of the incorporation of $AgNO_3$ into the RLB which decreased the energy band gap. The decreased energy band gap was due to emergence of new functional group and crystallite size which invariably makes Ag@RLEBN to have a better catalytic ability than RLB [1].

$$\alpha h\nu = K(h\nu - E_g)^{1/2} \qquad 2$$

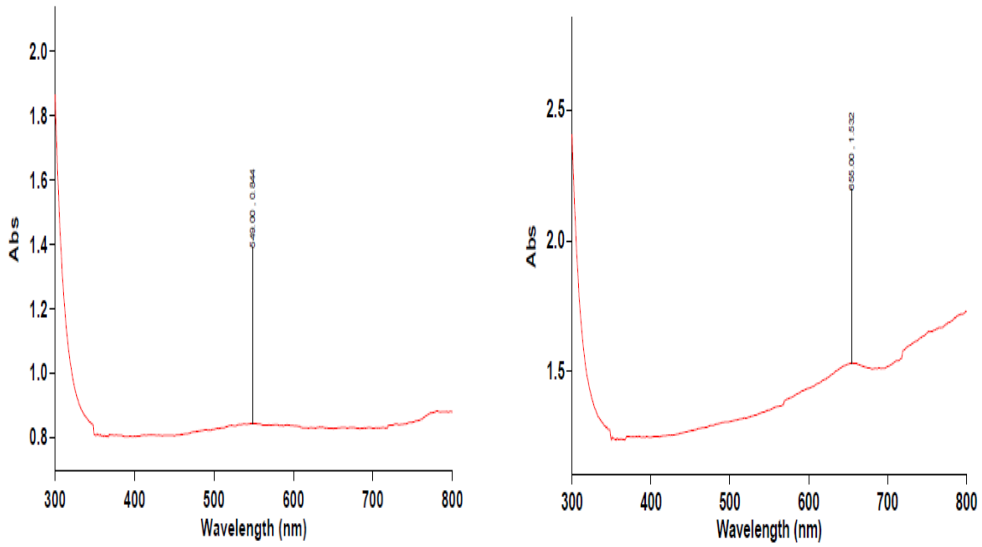


**Figure 3.** UV Visible spectroscopy of (A) RLB (B) Ag@RLEBN

### 3.4 SEM/EDX analysis of RLB, Ag@RLEBN and MB Loaded Ag@RLEBN

The SEM micrograph showing the morphological structure of RLB, Ag@RLEBN and MB loaded Ag@RLEBN is shown in Figure 4 A, B, C. From the SEM images, RLB shows clearly defined spheres that are well and homogenously distributed. A clear view of Ag@RLEBN indicates that the nanocomposite is rough, with white patches not formerly in RLB, uneven and composed of agglomerates of uniformly aggregated 3.21 % $AgNO_3$ nanoparticles. The surface of Ag@RLEBN is jagged with innumerable voids with increased porosity, stability and multifunctionality [22].

Evaluating the EDX of RLB, Ag@RLEBN and MB loaded Ag@RLEBN (Figures 5A, B and C) shows the appearance of strong signals for silver at 0.4 and 4.0 keV (Figure 5 B) and is consistent with other studies [20]. The zero-valent Ag in Ag@RLEBN (3.21%) was close to the silver ions initially dispersed on RLB (3.84 %) during the phytofabrication. Therefore, an indication of the effectiveness of rice leaf extract in the biogenic reduction of Ag ions to form AgNPs and a confirmation of the synergistic role [18].

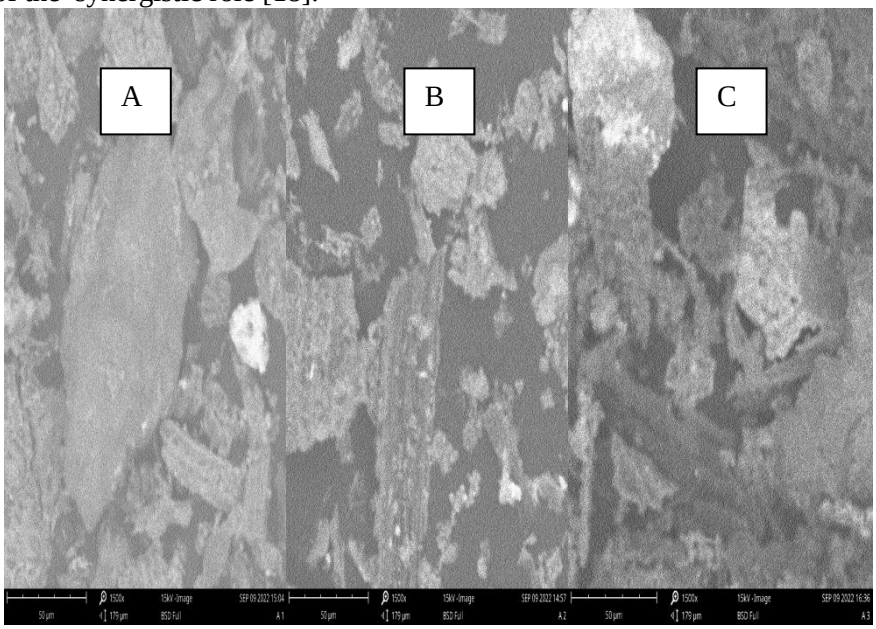


**Figure 4.** SEM micrograph of (A) RLB (B) Ag@RLEBN (C) MB loaded Ag@RLEBN

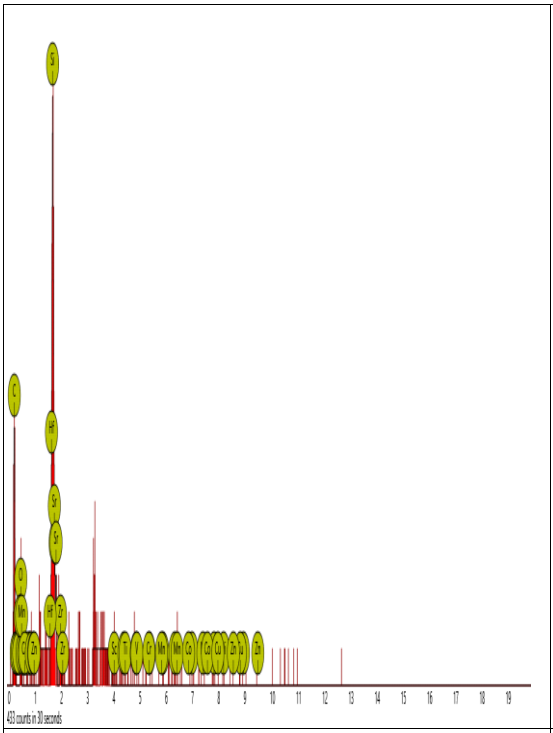

| Element Number | Element Symbol | Element Name | Atomic Conc. | Weight Conc. |
|---|---|---|---|---|
| 6 | C | Carbon | 67.06 | 29.65 |
| 14 | Si | Silicon | 12.27 | 12.69 |
| 8 | O | Oxygen | 7.27 | 4.28 |
| 72 | Hf | Hafnium | 4.79 | 31.49 |
| 38 | Sr | Strontium | 2.76 | 8.90 |
| 40 | Zr | Zirconium | 1.08 | 3.62 |
| 26 | Fe | Iron | 0.93 | 1.92 |
| 28 | Ni | Nickel | 0.71 | 1.52 |
| 21 | Sc | Scandium | 0.64 | 1.07 |
| 30 | Zn | Zinc | 0.60 | 1.44 |
| 29 | Cu | Copper | 0.45 | 1.05 |
| 9 | F | Fluorine | 0.36 | 0.25 |
| 27 | Co | Cobalt | 0.28 | 0.61 |
| 22 | Ti | Titanium | 0.28 | 0.49 |
| 25 | Mn | Manganese | 0.20 | 0.40 |
| 24 | Cr | Chromium | 0.17 | 0.33 |
| 23 | V | Vanadium | 0.15 | 0.29 |

**Figure 5A.** EDX data of RLB

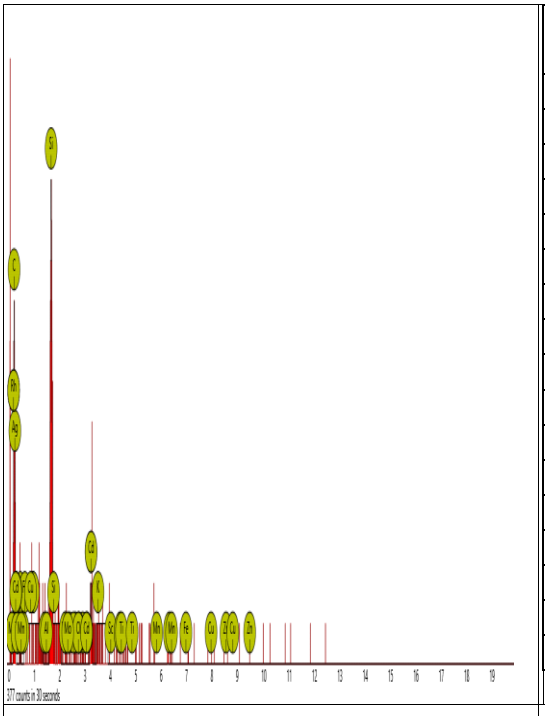

| Element Number | Element Symbol | Element Name | Atomic Conc. | Weight Conc. |
|---|---|---|---|---|
| 6 | C | Carbon | 74.70 | 49.43 |
| 14 | Si | Silicon | 9.00 | 13.93 |
| 8 | O | Oxygen | 6.49 | 5.72 |
| 19 | K | Potassium | 2.04 | 4.40 |
| 30 | Zn | Zinc | 1.61 | 5.79 |
| 26 | Fe | Iron | 1.53 | 4.72 |
| 16 | S | Sulfur | 0.64 | 1.12 |
| 29 | Cu | Copper | 0.60 | 2.11 |
| 13 | Al | Aluminium | 0.55 | 0.82 |
| 47 | Ag | Silver | 0.54 | 3.21 |
| 21 | Sc | Scandium | 0.49 | 1.20 |
| 45 | Rh | Rhodium | 0.46 | 2.63 |
| 42 | Mo | Molybdenum | 0.38 | 2.00 |
| 17 | Cl | Chlorine | 0.38 | 0.74 |
| 25 | Mn | Manganese | 0.26 | 0.79 |
| 22 | Ti | Titanium | 0.18 | 0.46 |
| 48 | Cd | Cadmium | 0.15 | 0.95 |

**Figure 5B.**EDX data of Ag@RLEBN

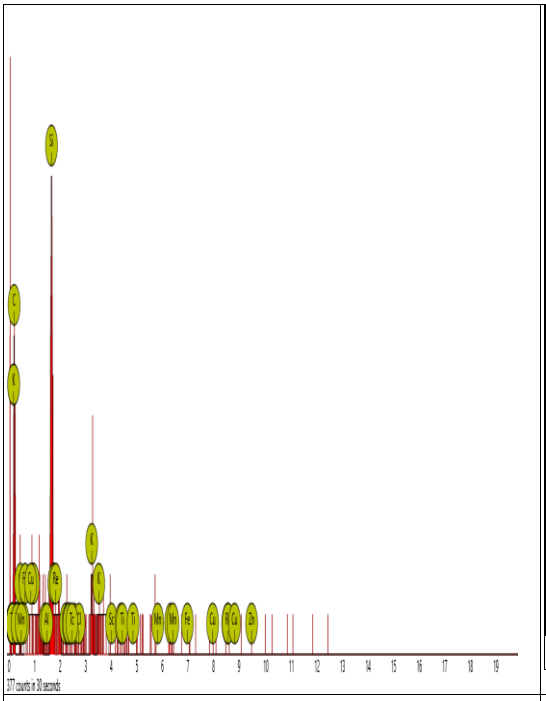

| Element Number | Element Symbol | Element Name | Atomic Conc. | Weight Conc. |
|---|---|---|---|---|
| 6 | C | Carbon | 73.03 | 36.73 |
| 14 | Si | Silicon | 8.97 | 10.55 |
| 8 | O | Oxygen | 4.89 | 3.28 |
| 75 | Re | Rhenium | 3.73 | 29.07 |
| 19 | K | Potassium | 2.27 | 3.72 |
| 30 | Zn | Zinc | 1.59 | 4.34 |
| 26 | Fe | Iron | 1.54 | 3.61 |
| 16 | S | Sulfur | 0.74 | 0.99 |
| 29 | Cu | Copper | 0.60 | 1.59 |
| 13 | Al | Aluminium | 0.52 | 0.59 |
| 21 | Sc | Scandium | 0.51 | 0.96 |
| 42 | Mo | Molybdenum | 0.44 | 1.75 |
| 17 | Cl | Chlorine | 0.43 | 0.64 |
| 43 | Tc | Technetium | 0.30 | 1.21 |
| 25 | Mn | Manganese | 0.26 | 0.60 |
| 22 | Ti | Titanium | 0.18 | 0.36 |

**Figure 5C.** EDX data of MB-loaded Ag@RLEBN

### 3.5 Effect of Initial Ag@RLEBN Concentration

The effect of intial concentration of Ag@RLEBN at 60 min and dosage of 0.005g (Figure 6) was evaluated by varying the concentration from 0.0001 to 0.1 M. The degradation of MB was highest at 0.0001M and a regress was observed afterwards. The increase in degradation typifies the availability of active sites where the molecules of the MB can cling to and the photons can easily access or penetrate facilitating the degradation [22]. The regress in the degradation efficiency could be attributed to the increased concentration of MB which altered effective and efficient penetration of photon to the surface of the photocatalyst.

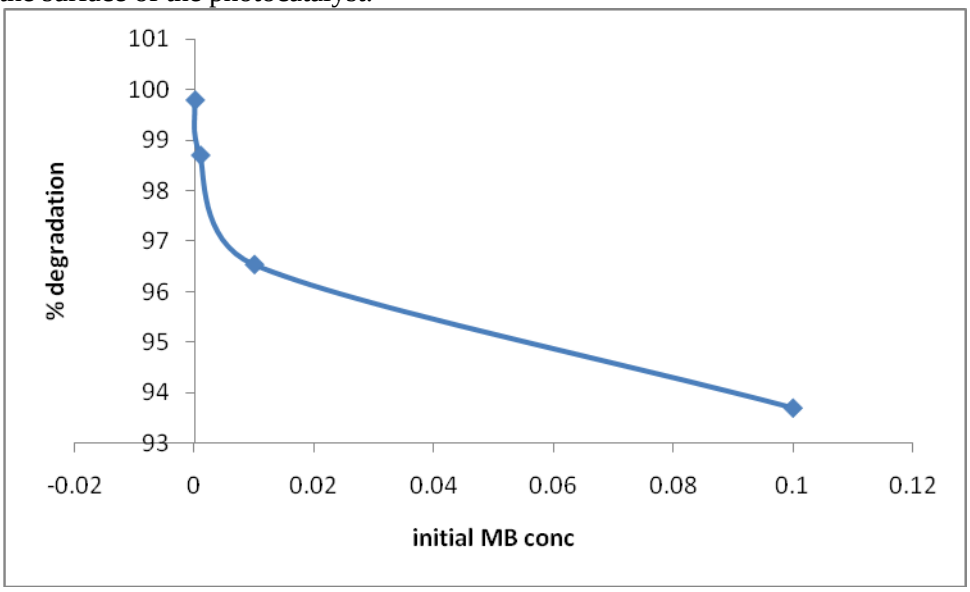


**Figure 6.** Effect of initial MB concentration on the photocatalytic degradation

### 3.6 Effect of Contact Time on the Photocatalytic Degradation of MB and Kinetic Studies

The contact time was varied between 20 to 100 min, fixed dosage of 0.005g and initial concentration of of MB of 0.001M (Figure 7). The degradation was highest at 60 min (97.95%) and

continued downwards to 100 min where the degradation was lowest (83.48 %). The high percentages of degradation suggest that the nanocomposite is capable of efficiently breaking down MB over time. The high percentages of degradation of MB across the different time intervals as shown in Figure 6 indicate that the Ag@RLEBN consistently exhibits strong photocatalytic propensity. The synergistic effect of the Ag-*rice* leaf extract nanoparticle and biochar could actually be implicated as responsible for the increased photocatalytic degradation efficiency. In comparison with other studies 1 involving Ag@biochar nanocomposite of *Chenopodium ambrosioides* leaf extract and biomass discovery was made that the time for highest degradation of MB for the present work is lower establishing a higher stability. From the kinetic point of view, the rate constant was evaluated as 0.248 $min^{-1}$ (Figure 7B) which was very close to values of phytosynthesized Ag@nanocomposite as well as chemically synthesized AgNPs which are 0.0147 and 0.011 $min^{-1}$ respectively1. The fabricated Ag@RLEBN could be the source of the electrons and hydroxyl free radicals which induces the photodegradation of MB. Therefore, Ag@RLEBN based on these results of high degradation rates observed.can be effective in the environmental remediation, such as water treatment or wastewater remediation.

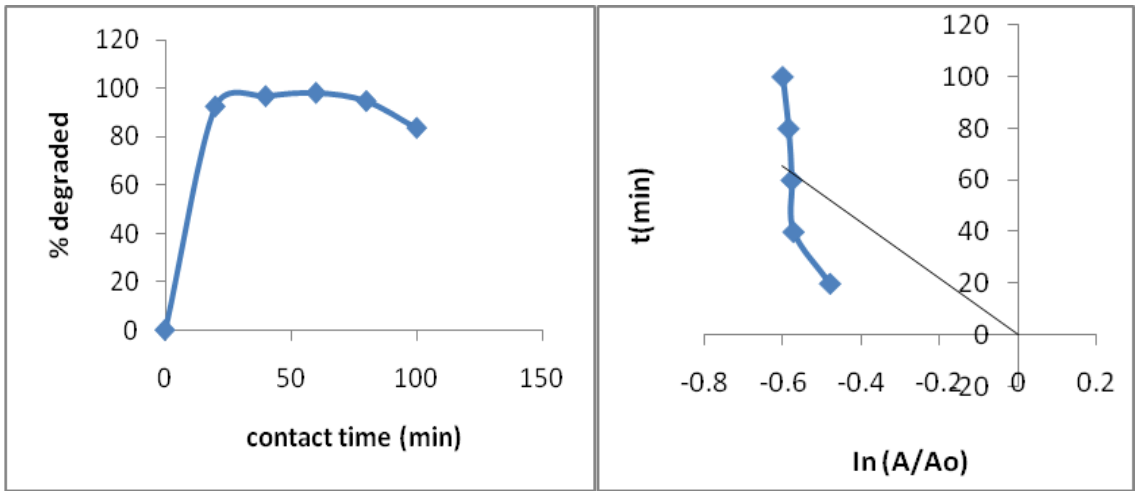


**Figure 7.** (A) Effect of contact time on MB degradation (B) kinetics of MB degradation Photocatalytic degradation of methylene blue

### 3.7 Effect of Dosage of Ag@RLEBN

The impact of Ag@RLEBN on MB degradation was studied using different doses of the photocatalyst at range of 0.001 to 0.008g, 60 min of activity and 0.001M solution of MB (Figure 8 ). Increase in the photocatalyst dose from 0.001g to 0.005g increased the photocatalytic degradation owing to the availability of active sites which experienced a regress at 0.006g. The decrease at higher doses of the photocatalyst could be attributed to the blocking of available spaces for effective light penetration [24-25].

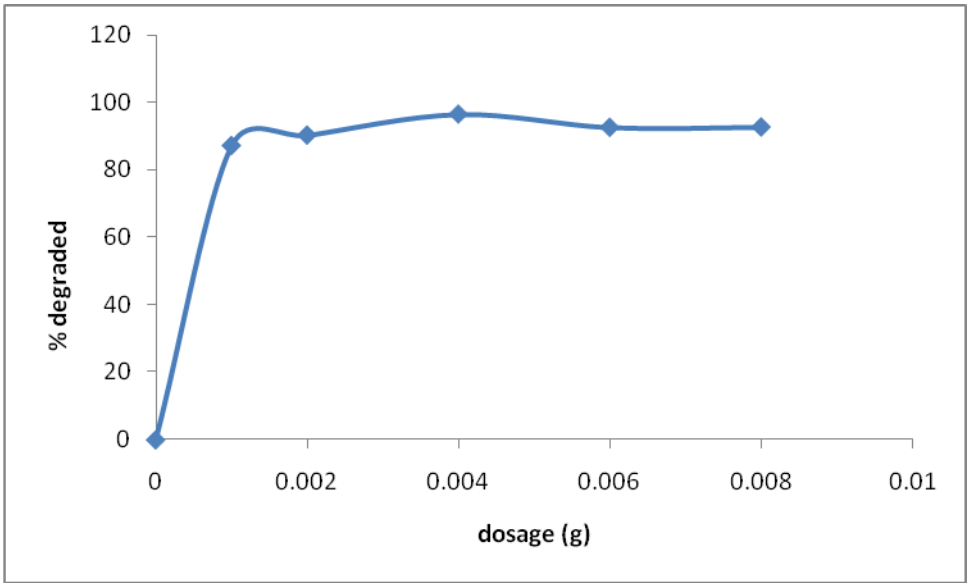


**Figure 8.** Effect of dosage on the degradation of MB

### 3.8 Reusability of Ag@RLEBN

Reusability of Ag@RLEBN was evaluated and after five cycles of reuse as shown in Figure 9, it was discovered that degradation ability only decreased by 2.05%. The decrease could be as a result of the alteration in the physical characteristics of Ag@RLEBN and other coagulating interferences [26].

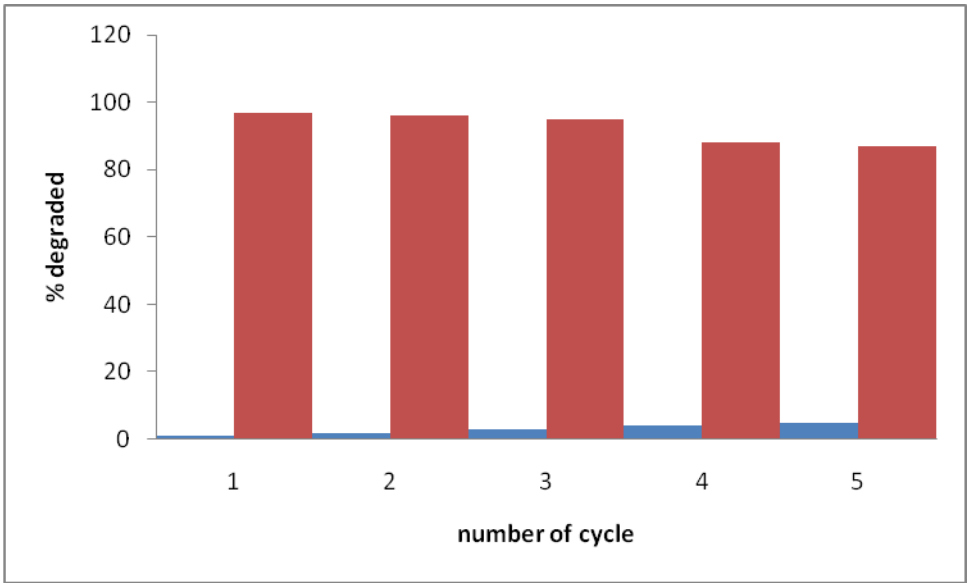


**Figure 9.** Reusability of the nancomposite

### 3.9 Mechanism of MB Removal Using Ag@RLEBN

Functionalization of RLB to form Ag@RLEBN increases the removal of MB since cationic dyes exhibit greater tendencies to adsorb onto the surface of negatively charged surfaces through electrostatic attraction, complexation, cationic exchange, π–π, n–π, and hydrogen bonding between the MB and OH groups present in Ag@RLEBN surface. Fast electron transfer processes and AgO in Ag@RLEBN could aid the photocatalytic degradation of MB within visible-light region [1,26-27]**.**
Electron holes are generated and reactive oxygen species mainly the OH radicals are liberated through the reaction free electrons with $O_2$ and $h^+$ with $H_2O$ molecules on the surface of Ag@RLEBN [1-3]. The mechanistic degradation of MB could be shown in Eqs 3 to 6.

$$e^- + O_2 \rightarrow * O_2^- \quad (3)$$

$h^+ + H_2O \rightarrow H^+ + {}^*OH$ (4)

$O_2$ + hv (visible) → $^1O_2$ (5)

$^* O_2^- + OH + {}^1O_2$ + MB → $CO_2 + H_2O$ + $Byproducts$ (6)

On careful comparism of the effectiveness of Ag@RLEBN to other photoctalyst as shown in Table 1, it was discovered that Ag@RLEBN is highly effective and efficient in the degradation of MB

**Table 1.** Comparison of degradation ability of Ag@RLEBN with other fabricated nanocomposites

| Catalyst | Photodegradation Capacity (%) | Dye Conc (Mg/L) | Time (min) | References |
|---|---|---|---|---|
| AgNPs | 82.8 | 60 | 180 | 21 |
| Ag/ZnO | 81.2 | 25 | 240 | 24 |
| Ag/ZnO nanocomposite | 94.3 | 10 | 120 | 26 |
| Ag@biochar nanocomposite | 88.4 | 25 | 75 | 1 |
| Ag@RLEBN | 98.70 | 25 | 20 | this work |

### 3.10 Antimicrobial Evaluation of Ag@RLEBN

The interaction between the proposed antimicrobial agentsb Ag@RLEBN involves the liberation of reactive oxygen species (ROS) (hydroxyl radical, hydrogen peroxide, superoxide ion) upon contact with the cell walls of the microbes [3,16]. Comparison of the effectiveness of Ag@RLEBN with similar phytofabricated nanocomposites (Table 2, Plate 1) indicates that it could serve as an antimicrobial agent for the decimation of .*staph aureus, salmonella spp and klebsiella.* The inability of Ag@RLEBN to be effective against *E.coli* could be as a result of lack of penetration into the cell wall of the microorganisms [5].

**Table 2.** Comparison between the antimicrobial efficacy of the nanocomposite and other nanocomposites

| Sample | Concentration ($mg/mL^{-1}$) | Bacterial Strain | Microbial Zone of Inhibition (mm) | References |
|---|---|---|---|---|
| Ag/GO nanocomposite | 1 | *Staph aureus*<br>*E. coli* | 15<br>19 | 28 |
| copper/silver titanium oxide nanocomposite (Cu-Ag-$TiO_2$) | 0.5 | *Staph*<br>*E.coli* | 21<br>16 | 3 |
| Ag@biochar nanocomposite | 1 | *Staph*<br>*E.coli*<br>*Klebsiella* | Resistant<br>No growth<br>18 | 1 |
| AgNp embedded guar gum/gelatin nanocomposite | 0.5 | *Staph*<br>*E.coli*<br>*Pseudomonia aeuroginosa* | 13<br>12.5<br>12 | 5 |
| Ag@RLEBN | 0.5 | *Staph*<br>*E.coli*<br>*Klebsiella*<br>*salmonella* | 08<br>---<br>12<br>10 | This work |

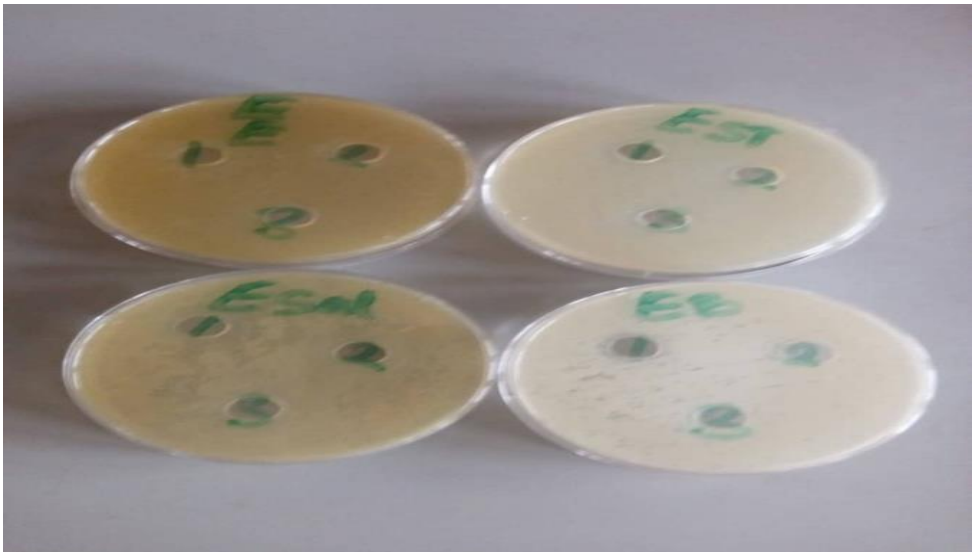

**Figure 10.** Antimicrobial inhibition zone diameter of Ag@RLEBN

## 4. Conclusion

Facile green hydrothermal techniques was applied in this study for the phytofabrication of simple, ecofriendly and low cost biogenic Ag@ rice leaf extract-biochar nanocomposite. The synthesized nanocomposite was used for the photocatalytic removal of methylene blue and microorganism from water samples. The nanocomposite excellent bioreduction of Ag ions was shown in SEM/EDX data. The photodegradation of methylene blue using the nanocomposite indicated 99.7% removal at initial concentration of 0.0001M. Evaluating the antimicrobial potency of the new organic-inorganic hybrid material indicated elevated zone of inhibition for *staph aureus, salmonella spp and klebsiella*. The nanocomposite is effective, effeicient ecofriendly, low cost, synthetically replicable and can be used for environmental sanitization

## Acknowledgment

The authors acknowledge the laboratory technicians of microbiology department Ebonyi State University, Abakaliki for helping with antimicrobial analysis

## References

[1] S.E.Abdelazeem, M.A. Ahmed,, H. Mohamed and F. Manal. (2022). Novel Biogenic Synthesis of a Ag@Biochar Nanocomposite as an Antimicrobial Agent and Photocatalyst for Methylene Blue Degradation .ACS Omega. 9 pp 8046-8059

[2] P. Balaji, K. Bhuvaneswari, M. Indrani, S. Mohamad, N.A. Alsalhi, T. Pazhanivel and P. Sakthivel (2023).Designing the heterostructured FeWO4/FeS2 nanocomposites for an enhanced photocatalytic organic dye degradation..*Chemosphere. 334* pp138979

[3] M.Ghosh, S. Mandal, A. Roy, A. Paladhi, P. Mondal, S. Hira, S. Mukhopadhyay and S.K.Pradhan,(2021). Synthesis and characterization of a novel drug conjugated copper- silver-titanium oxide nanocomposite with enhanced antibacterial activity .J. Drug Delivery Sci. Technol.. 62pp102384

[4] Y. Tan, Y. Liu and H. Gu.(2016). Biochar-based nano-composites for the decontamination of wastewater: a review. Bioresour. *Journal of Technology.* 212(1) pp318–333

[5] N. Khan, D. Kumar and P. Kumar. (2020).Silver nanoparticles embedded guar gum/gelatin nanocomposite: Green synthesis, characterization and antibacterial activity Colloid Interface Sci. Commun.. 35 pp100242

[6] F.S. Nworie, F.I. Nwabue, W. Oti, E. Mbam and B.U. Nwali.(2019). Removal of Methylene Blue from Aqueous Solution Using Activated Rice Husk Biochar: Adsorption Isotherms, Kinetics and Error analysis. *Journal of the Chilean Chemical Society* .64(1),pp4365-4376

[7] H. Yousaf, A, Mehmood, K.S. Ahmad and M. Raffi. (2020).Green synthesis of silver nanoparticles and their applications as an alternative antibacterial and antioxidant agents. Mater. Sci. Eng., C 112 pp110901

[8] G. Aayush, K.A. Kajal, K. Loveleen, O.P. Brar and P.R. Pandey. (2024).Facile synthesis of Mn3O4–ZnO composite for photocatalytic dye removal and capacitive applications *Materials Chemistry and Physics .313* pp 128698

[9] J. Cheng, C. Zhan, J. Wu, Z. Cui, J. Si, Q. Wang, X. Peng and L.S. Turng.(2020). Highly Efficient Removal of Methylene Blue Dye from anAqueous Solution Using Cellulose Acetate Nanofibrous Membranes Modified by Polydopamine *ACS Omega* .55pp 5389– 5400

[10] T.G. Fikadu, A.K. Mesfin, W.S. Megersa M.A., Dinsefa, A.T. Newayemedhin, and G.H. Fekadu.(2023). Facile synthesis of different metals doped α-PbO nanoparticles for photocatalytic degradation of Methylene Blue dye *Physica Scripta*, *98* (6) pp 065701

[11] W.M. Fong, A.C. Affam, and Chung.(2020). Synthesis of Ag/Fe/CAC for colour and COD removal from methylene blue dye wastewater. *International Journal Environment Science Technology.* 17pp 3485–3494

[12] M. Ahmad, W. Rehman, M.M. Khan, M.T. Qureshi, A. Gul, S. Haq, R. Ullah, A. Rab, and F Menaa.(2021). Journal *Environment Chemical Engineer.* 69pp 104-725

[13] N. Mohammed , H.K. Jae, L. Hee-Young and K.C. Sung .(2021). Development of Three-Dimensional Nickel–Cobalt Oxide Nanoflowers for Superior Photocatalytic Degradation of Food Colorant Dyes: Catalyst Properties and Reaction Kinetic Study .*Langmuir 37* (44) pp 12929-129399

[14] H. Ahmed, A.S.A. Naggar, T.A. Ahmed and N.F. Seaf El-Nasr.(2023). Phytogenic fabrication of ZnO and gold decorated ZnO nanoparticles for photocatalytic degradation of Rhodamine B *Inorganics. 11* (12) pp 484

[15] A. Akbarzadeh, L. Kafshdooz, Z. Razban, T.A. Dastranj, S. Rasoulpour, R. Khalilov, T. Kavetskyy, S. Saghfi, A.N. Nasibova, S. Kaamyabi and T. Kafshdooz. .(2018). An overview application of silver nanoparticles in inhibition of herpes simplex virus. Nanomed Biotechnol .46(2),pp263-267

[16] P. Panchal, D.R. Paul, A. Sharma, P. Choudhary, P. Meena and S.P. Nehra.(2020). Biogenic mediated Ag/ZnO nanocomposites for photocatalytic and antibacterial activities towards disinfection of water J. Colloid Interface Sci.. 563pp370−380

[17] S. Payel and D. Debajyoti. (2023).ZnO-Nanorod/$Ag_2O$-Nanoparticle/rGO-Nanosheet Heterostructures as Photocatalysts for Enhanced Degradation of Harmful Aqueous Phase Contaminants under Extended Visible Light Exposure *ACS Applied Nano Materials .6* (24) pp 22730-22744

[18] S. Mustafa, B. Filiz and O. Merve. (2023).Treatment of Automotive Paint Wastewater: Photocatalytic degradation of methylene blue using semi-conductive $ZrO_2$ *International Journal of Automotive Science and Technology .7* (4) pp316- 324

[19] M. Nima, D. Reza, F. Masoud, B. Morteza and E.K.Mahmoud..(2024). Anodizing of commercial galvanized mesh followed by electroless decorating of Ag nanoparticles for application as novel and low-cost photocatalyst for degradation of both dye and microbiological pollutants. *Journal of Photochemistry and Photobiology A: Chemistry. 447* pp115257

[20] Z. Zakarya, D. Nadra and S. Tahar (2024).Sheet-like g-C3N4 for enhanced photocatalytic degradation of naproxen *Journal of Photochemistry and Photobiology A: Chemistry .446* pp 115189

[21] A.A.Fairuzi, N.N.Bonnia, R.M. Akhir, M.A. Abrani and H.M. Akil.(2018). Degradation of methylene blue using silver nanoparticles synthesized from imperata cylindrical aqueous extract IOP Conf. Ser. Earth Environ. Sci. 105 pp 012018

[22] F. M. Sanakousar, C. Vidyasagar, D.B. Shikandar, M. Victor. M. Jiménez Pérez, C. Viswanath, and K. Prakash ..(2024).Thermal decomposition synthesis of cylindrical rod-like $MoO_3$ and irregular sphere-like $Ag_2MoO_4$ nanocrystals for accelerating photocatalytic degradation of industrial reactive dyes and biosensing application. *Journal of Environmental Chemical Engineering. 11* (2) pp 109371

[23] F.S .Nworie, F.I. Nwabue and E. Nwoke.(2024). Activated multifunctional nanoparticle biochar for highly efficient capture and removal of Ni(II) and micro-organisms from water samples Int. J. Environment and Waste Management . 33(4),pp 422–437

[24] J. Singh and A.S. Dhaliwal. (2020). Plasmon-induced photocatalytic degradation of methylene blue dye using biosynthesized silver nanoparticles as photocatalyst Environ. Technol.. 41pp 1520−1534

[25] R.R. Dibya and M.J.Hara. (2023).Facile synthesis of novel Z-scheme GO-modified ternary composite as photocatalyst for enhanced degradation of bisphenol-A under sunlight *Journal of the Taiwan Institute of Chemical Engineers .147* pp104914

[26] M.F. Abdel Messih, M.A. Ahmed, A. Soltan, and S.S. Anis. (2019).Synthesis and characterization of novel Ag/ZnO nanoparticles for photocatalytic degradation of methylene blue under UV and solar irradiation J. Phys. Chem. Solids. 135pp 109086

[27] C.B.P. Suresh, S.D. Maneesha, D. Kailash, S. Dilip, S.S. Koyal, K.. Vaishnavi, D. Arup, S. Somaditya. (2024).Enhanced photocatalytic degradation of organic pollutants in water using copper oxide (CuO) nanosheets for environmental application. S *JCIS Open*, *16* pp100102

[28] J.E. Jeronsia, R. Ragu, R. Sowmya, A. Mary. (2024).Comparative investigation on Camellia Sinensis mediated green synthesis of Ag and Ag/GO nanocomposites for its anticancer and antibacterial efficacy Surf. Interfaces . 21,pp100787..